



# 1 Aerosol and dynamical contributions to cloud droplet formation 2 in Arctic low-level clouds

3 Ghislain Motos<sup>1</sup>, Gabriel Freitas<sup>2,3</sup>, Paraskevi Georgakaki<sup>1</sup>, Jörg Wieder<sup>4,†</sup>, Guangyu Li<sup>4</sup>, Wenche  
4 Aas<sup>5</sup>, Chris Lunder<sup>5</sup>, Radovan Krejci<sup>2,3</sup>, Julie T. Pasquier<sup>4,‡</sup>, Jan Henneberger<sup>4</sup>, Robert O. David<sup>6</sup>,  
5 Christoph Ritter<sup>7</sup>, Claudia Mohr<sup>2,3,¶</sup>, Paul Zieger<sup>2,3</sup>, Athanasios Nenes<sup>1,8</sup>

6 <sup>1</sup>Laboratory of Atmospheric Processes and their Impacts, School of Architecture, Civil & Environmental Engineering,  
7 École Polytechnique Fédérale de Lausanne, Lausanne, Switzerland

8 <sup>2</sup>Department of Environmental Science, Stockholm University, Stockholm, Sweden

9 <sup>3</sup>Bolin Centre for Climate Research, Stockholm University, Stockholm, Sweden

10 <sup>4</sup>Department of Environmental Systems Science, Institute for Atmospheric and Climate Science, ETH Zurich, Zurich,  
11 Switzerland

12 <sup>5</sup>NILU—Norwegian Institute for Air Research, Kjeller, Norway

13 <sup>6</sup>Department of Geosciences, University of Oslo, Oslo, Norway

14 <sup>7</sup>Alfred Wegener Institute, Helmholtz Centre for Polar and Marine Research, Potsdam, Germany

15 <sup>8</sup>Center for the Study of Air Quality and Climate Change, Institute of Chemical Engineering Sciences, Foundation for  
16 Research and Technology Hellas, Patras, Greece

17 <sup>†</sup>now at: femtoG AG, Zurich, Switzerland

18 <sup>‡</sup>now at: Meteomatics AG, St. Gallen, Switzerland

19 <sup>¶</sup>now at Laboratory of Atmospheric Chemistry, Paul Scherrer Institute, Villigen, Switzerland

20 *Correspondence to:* Ghislain Motos ([ghislain.motos@epfl.ch](mailto:ghislain.motos@epfl.ch)), Athanasios Nenes ([athanasios.nenes@epfl.ch](mailto:athanasios.nenes@epfl.ch))

21 **Abstract.** The Arctic is one of the most rapidly warming regions of the globe. Low-level clouds and fog modify the  
22 energy transfer from and to space and play a key role in the observed strong Arctic surface warming, a phenomenon  
23 commonly termed "Arctic amplification". The response of low-level clouds to changing aerosol characteristics  
24 throughout the year is therefore an important driver of Arctic change that currently lacks sufficient constraints. As  
25 such, during the NASCENT campaign (Ny-Ålesund AeroSol Cloud Experiment) extending over a full year from  
26 October 2019 to October 2020, microphysical properties of aerosols and clouds were studied at the Zeppelin station  
27 (475 m a.s.l.), Ny-Ålesund, Svalbard, Norway. Particle number size distributions obtained from differential mobility  
28 particle sizers as well as chemical composition derived from filter samples and an aerosol chemical speciation monitor  
29 were analyzed together with meteorological data, in particular vertical wind velocity. The results were used as input to  
30 a state-of-the-art cloud droplet formation parameterization to investigate the particle sizes that can activate to cloud  
31 droplets, the levels of supersaturation that can develop, the droplet susceptibility to aerosol and the role of vertical  
32 velocity. We evaluate the parameterization and the droplet numbers calculated through a droplet closure with in situ  
33 measurements. A remarkable finding is that, for the clouds sampled in situ, closure is successful in mixed-phase cloud  
34 conditions regardless of the cloud glaciation fraction. This suggests that secondary ice production through ice-ice  
35 collisions or droplet-shattering may explain the high ice fraction, as opposed to rime-splintering that would  
36 significantly reduce the cloud droplet number below levels predicted by warm cloud activation theory. We also show  
37 that pristine-like conditions during fall led to clouds that formed over an aerosol-limited regime, with high levels of  
38 supersaturation (generally around 1%, although highly variable) that activate particles smaller than 20 nm in diameter.  
39 Clouds formed in the same regime in late spring and summer, but aerosol activation diameters were much larger due



40 to lower cloud supersaturations (c.a. 0.5%) that develop because of higher aerosol concentrations and lower vertical  
41 velocities. The contribution of new particle formation to cloud formation was therefore strongly limited, at least until  
42 these newly formed particles started growing. However, clouds forming during the Arctic haze period (winter and early  
43 spring) can be limited by updraft velocity, although rarely, with supersaturation levels dropping below 0.1% and  
44 generally activating larger particles (20 to 200 nm), including pollution transported over a long range. The relationship  
45 between updraft velocity and the limiting cloud droplet number agrees with previous observations of various types of  
46 clouds worldwide, which tends to confirm the universality of this relationship.

## 47 **1 Introduction**

48 Greenhouse gas-induced warming is affecting the Arctic more than any other region on the planet (Rantanen et al.,  
49 2022). Arctic aerosols have been shown to partially offset local surface warming (Najafi et al., 2015; Breider et al.,  
50 2017), which is already impacting the region (Vincent, 2020). Their capacity to form clouds and subsequently impact  
51 shortwave and longwave radiation fluxes can strongly influence the regional surface albedo, surface radiation budget,  
52 and thus the melting of snow and sea ice (e.g. Curry et al., 1996; Maturilli et al., 2015). Low-level clouds influence the  
53 Arctic climate in a substantial but complex manner, with either a positive or a negative forcing depending on the season  
54 and the latitude (Intrieri et al., 2002; Shupe and Intrieri, 2004; Tjernström et al., 2014; Tan and Storelvmo, 2019).  
55 Arctic low-level clouds are frequently mixed-phase (e.g. Shupe et al., 2008), which makes their representation in  
56 models and understanding of their response to cloud condensation nuclei (CCN) availability highly challenging,  
57 although critical for understanding Arctic change (e.g., Seinfeld et al., 2016; Sotiropoulou et al., 2016). Extensive long-  
58 term observations of aerosols and clouds have been performed in the Arctic (e.g., Platt et al., 2022; Koike et al., 2019);  
59 however, aerosol-cloud interactions, and in particular cloud droplet formation processes have to be understood to  
60 comprehend the rapid changes occurring in this region of the world. Furthermore, droplet formation and concentrations  
61 in mixed-phase clouds (MPCs) are rarely evaluated, even though they can have a profoundly important impact on MPC  
62 properties and evolution.

63 Ny-Ålesund, a scientific settlement based in the Svalbard archipelago, offers a remarkable location for studying the  
64 Arctic atmosphere and processes related to aerosol-cloud interactions, with stations located both at sea level and on  
65 Zeppelin mountain (475 m a.s.l.). As in the rest of the Arctic, clouds are ubiquitous at Ny-Ålesund, being present 81%  
66 of the time (Nomokonova et al.; 2019) with a majority of MPCs, as confirmed by Lawson et al. (2011) over the spring  
67 season using a tethered-balloon system. 90% of these MPCs are located below an altitude of 3000 m (Mioche et al.,  
68 2015). A combination of ground-based remote sensing observations of cloud properties and the application of  
69 broadband radiative transfer simulations allowed to conclude that clouds have an overall warming effect on the surface  
70 at Ny-Ålesund (annual average of  $11.1 \text{ W m}^{-2}$ ), although the net surface cloud radiative effect is negative in summer  
71 and positive the rest of the year (Ebell et al., 2020). Ny-Ålesund, owing to both its orographic and maritime landscapes,  
72 may also bear atmospheric characteristics that are different from the rest of the Arctic (Maturilli et al., 2019). For  
73 example, Mioche et al. (2015) showed that mixed-phase clouds (MPCs) are present around 55% of the time above Ny-  
74 Ålesund, whereas in the rest of the Arctic, the mean frequency of occurrence is 30% in the winter and 50% for the rest  
75 of the year.



76 Regarding aerosol size distribution, although no site was shown to be representative of the whole Arctic, several  
77 features, such as number concentrations and dominant mode of the size distribution throughout the year, are common  
78 to Zeppelin and other Arctic sites such as Nord (Greenland), Barrow (Alaska) or Tiksi (Siberia), as shown by Croft et  
79 al. (2016) or Freud et al. (2017). Differences to other Arctic stations can be partly related to Zeppelin being located  
80 close to the European continent and to open ocean or in the free troposphere (FT; Ström et al., 2009). Nevertheless, a  
81 topography analysis suggested that Zeppelin is influenced to a large extent by planetary boundary layer (PBL) air  
82 masses (Collaud Coen et al., 2018). Di Liberto et al. (2012) have shown that over a spring day (with no sunset), the  
83 station resided in the PBL from 04:00 to 16:00 and in the FT the rest of the day. Such a diurnal cycle is typically  
84 observed in lower latitude and higher altitude sites (Collaud Coen et al., 2018).

85 Seasonal patterns of aerosol concentrations and size distributions at the Zeppelin station have been extensively  
86 investigated (e.g. Ström et al., 2003; Tunved et al., 2013; Croft et al., 2016). The results agree towards a minimum in  
87 number concentration at the onset of fall due to efficient cloud scavenging, scarce transport from lower latitudes and  
88 limited new particle formation. Concentrations then increase constantly until they reach the spring Arctic haze  
89 maximum. The accumulation mode is dominant over this period, until it gets efficiently scavenged in summer, and the  
90 Aitken mode then becomes dominant, due to active new particle formation favoured by strong solar radiation and the  
91 absence of condensational sinks (Dall'Osto et al., 2017; Park et al., 2021).

92 The seasonality of CCN at Zeppelin tends to follow that of the aerosol particle number concentration (Jung et al., 2018;  
93 Koike et al., 2019). Using a counterflow virtual impactor inlet, Karlsson et al. (2021) showed that cloud residuals also  
94 follow the same seasonality, but negative temperatures cause cloud residual concentrations to drop compared to aerosol  
95 concentration. The dominant Aitken mode in summer does not cause a drop in the number of CCN and cloud residuals,  
96 suggesting that also particles down to 20 nm in diameter can activate to cloud droplets during this season (Leitch et  
97 al., 2016; Karlsson et al., 2021). Using aircraft measurements over Alaska, Moore et al. (2011) also showed that most  
98 aerosols can act as CCN at supersaturations above 0.1% in this region, i.e. where only particles larger than around 100  
99 nm are generally able to activate to cloud droplets. Gramlich et al. (2022) came to the same conclusion by performing  
100 chemical analyses of aerosol particles and gases before, during and after cloud, without noting strong variations in  
101 chemical composition. CCN are typically associated with accumulation mode particles; however, much smaller  
102 particles can activate to cloud droplets if the supersaturations developed in clouds are high enough. Using an adiabatic  
103 cloud parcel model, Pöhlker et al. (2021) proposed that in clean environments, such as the Arctic, Aitken mode particles  
104 can act as CCN at low updraft velocities (below  $1 \text{ m s}^{-1}$ ). Similarly, Bulatovic et al. (2021) reported a strong influence  
105 of Aitken mode particles on the subsistence of stratiform Arctic mixed-phase clouds.

106 In the atmosphere, supersaturated air associated with cloudy airmasses leads to the unconstrained condensation of  
107 water vapour on CCN, leading to cloud droplet activation. The main mechanism driving this process is expansion  
108 cooling of ascending air parcels (e.g. Nenes et al., 2001). Droplet number, however, depends on a combination of the  
109 cooling and aerosol forming droplets, either of which can be a "limiting factor", eventually controlling the cloud  
110 susceptibility to aerosol. If the factor limiting droplet formation is the lack of aerosol particles (this is the "aerosol-  
111 limited" regime), the droplet concentration is directly proportional to the aerosol number concentration and is  
112 effectively independent of updraft velocity. The opposite situation can occur, giving rise to an "updraft-limited" regime  
113 (e.g. Jensen and Charlson, 1984; Twomey, 1993) during which cloud droplet formation is insensitive to any further



114 increase in aerosol concentration. Between these two limiting cases, it is expected that a transitional regime also exists,  
115 for which cloud droplet formation is sensitive to both updraft velocity and aerosol properties (Reutter et al., 2009).  
116 Given the influence of cloud droplet number on cloud radiative effects, knowledge of the prevalent droplet formation  
117 regime in various regions of the world and how it varies throughout the year is of primary importance, because it  
118 determines the type of optimal constraints (dynamical or aerosol) required in models. Few studies have used this  
119 perspective to determine the best observational results for reducing model uncertainties. Regarding the aerosol-CCN-  
120 droplet link, several studies focusing on the Arctic have reported that periods of aerosol-limited regime are frequently  
121 found (Garrett et al., 2004; Mauritsen et al., 2011; Eirund et al., 2019), but these studies do not cover a whole year,  
122 and/or do not fully constrain the aerosol and updraft velocity characteristics and their relation to cloud supersaturation,  
123 activated aerosol size, aerosol source/processes and limiting cloud droplet number (i.e., an asymptotic upper limit of  
124 droplet number). The Swiss Alps have been the most extensively studied region in that regard so far, using high-altitude  
125 ground-based measurements (Hammer et al., 2015; Hoyle et al., 2016; Georgakaki et al., 2021). At other locations,  
126 aircraft flights have been used to investigate cloud formation at higher altitudes, e.g., over the United States of America  
127 (Bougiatioti et al., 2020) and the southeastern Atlantic ocean (Kacarab et al., 2020).  
128 The Ny-Ålesund AeroSol Cloud Experiment (NASCENT) campaign took place from fall 2019 to fall 2020 over  
129 several sites located close to Ny-Ålesund, Svalbard. Pasquier et al. (2022) comprehensively describe the meteorological  
130 context, aerosol climatology, instrumental setup as well as first results related to aerosol-cloud interactions (for liquid,  
131 ice, and mixed-phase clouds). Here, we utilized in situ data collected during this campaign to feed a cloud droplet  
132 formation parameterization in order to unravel the sensitivity of cloud droplet number to aerosol concentration and  
133 composition as well as updraft velocity. Sect. 2 describes the NASCENT campaign and the instrumentation used to  
134 provide the data for this study. These data serve as input to the cloud droplet parameterization detailed in Sect. 3, where  
135 additional analyses linked to specific instruments are also described. In Sect. 4, parameterization outputs are exposed,  
136 analyzed and discussed in the broader context of the Arctic seasonal aerosol cycle, together with a droplet closure.  
137 Sect. 5 provides concluding remarks.

## 138 **2 Measurements**

### 139 **2.1 Measurement site and period**

140 The NASCENT campaign took place in the Svalbard archipelago (also known as Spitsbergen) close to the small seaside  
141 settlement of Ny-Ålesund from October 2019 to October 2020. Svalbard itself has  
142 very limited anthropogenic aerosol emissions, but it can be influenced by North Atlantic stormy air masses. In order  
143 to limit the influence of locally produced sea spray aerosols and make the results more regionally representative, a  
144 measurement station located on top of Mount Zeppelin (475 m a.s.l.; 78° 54' N, 11° 53' E), approximately two  
145 kilometers south of Ny-Ålesund, served as a sampling site for all data presented in this study, unless explicitly stated  
146 otherwise.



147 **2.2 Instrumentation**

148 **2.2.1 Particle number size distributions**

149 Two differential mobility particle sizers (DMPSs) continuously measured particle number size distribution at the  
150 Zeppelin station. In the DMPS, the aerosol is first electrically charged by a  $^{63}\text{Ni}$  source, allowing selection by electrical  
151 mobility, thus mobility diameter, by a differential mobility analyzer (DMA). Condensation particle counters (CPC,  
152 TSI models 3010 for DMPS\_1 and 3772 for DMPS\_2) then measure the concentration of particles contained in the  
153 monodisperse flow. The integration of the particle number size distribution between the boundaries of the measured  
154 size spectrum provides the integrated particle number concentration,  $N_{\text{aer}}$ . The DMPSs were connected to a whole-air  
155 inlet heated to a temperature of 5-10 °C, following the guidelines of the Global Atmosphere Watch (GAW) program  
156 of the World Meteorological Organization (WMO). The size range measured by both DMPSs were 20 to 775 nm for  
157 DMPS\_1 and 10 to 945 nm for DMPS\_2. DMPS\_1 and DMPS\_2 had a scanning duration of 11 and 7 min, respectively.  
158 The size distributions were corrected for particle losses in the inlet using the software tool developed by von der Weiden  
159 et al. (2009). More details on the DMPS setup at the Zeppelin station can be found in the study of Karlsson et al.  
160 (2021).

161 **2.2.2 Aerosol chemical composition**

162 The mass concentration of non-refractory bulk aerosol was measured by a time-of-flight aerosol chemical speciation  
163 monitor (ToF-ACSM; Fröhlich et al., 2013), whose technology is based on the aerosol mass spectrometer (AMS;  
164 Aerodyne Research Inc., Billerica, MA, USA). Measurements were also performed using a 3 stage filter pack system  
165 manufactured by the Norwegian Institute for Air Research (NILU) and designed for sampling of particles and gaseous  
166 compounds. The filters have a diameter of 47 mm and the flowrate is 12-16 L/min with a sampling duration of 24  
167 hours. First in the direction of the air flow is a Teflon filter (Millipore 3  $\mu\text{m}$ ) for collecting ions ( $\text{SO}_4^{2-}$ ,  $\text{NH}_4^+$ ,  $\text{NO}_3^-$ ,  
168  $\text{Ca}^{2+}$ ,  $\text{K}^+$ ,  $\text{Cl}^-$ ,  $\text{Na}^+$ ). This is followed by an alkaline (KOH) and an acid (oxalic acid) impregnated filters (Whatman 40)  
169 to collect respectively volatile acidic and alkaline components. These instruments sampled behind a whole-air inlet  
170 (with a size-cut of around 10  $\mu\text{m}$ , based on tests performed behind the inlet); note however that the TOF-ACSM uses  
171 a particulate matter larger than 2.5  $\mu\text{m}$  ( $\text{PM}_{2.5}$ ) aerodynamic lens. Organic carbon mass concentration was derived from  
172 filter samples collected by a Digital high-volume sampler with a  $\text{PM}_{10}$  inlet, which operated at a flow rate of 689 L/min  
173 over a whole week. The aerosol particles were collected on prefired (850 °C; 3 h) quartz fiber filters (PALLFLEX  
174 Tissuequartz 2500QAT-UP; 150 mm in diameter). Thermal-optical analysis (TOA) was performed using a Sunset Lab  
175 OC/EC Aerosol Analyzer, using transmission for charring correction, and operated according to the EUSAAR-2  
176 temperature program (Cavalli et al., 2010).  
177 Equivalent black carbon (eBC) concentration was retrieved from a multi-angle absorption photometer (MAAP, model  
178 5012, Thermo Fisher Scientific, Waltham, MA, USA). This instrument collects particles on a fiber filter and measures  
179 the transmission and back scattering of laser light at multiple angles to determine the aerosol absorption coefficient at  
180 a wavelength of 637 nm. eBC concentration, calculated from this coefficient using a mass absorption cross-section  
181 (MAC) value of 10.6  $\text{m}^2 \text{g}^{-1}$  (as suggested by Ohata et al., 2021), was used to complement both ACSM and filterpack  
182 data in order to retrieve aerosol hygroscopicity.



183 **2.2.3 Meteorological data**

184 Three dimensional wind was continuously observed with a 1 Hz ultrasonic anemometer (model uSonic-3 Omni,  
185 METEK GmbH, Elmshorn, SH, Germany), which was placed close to the whole-air inlet. The uSonic measures the  
186 speed of sound in between three pairs of transducers and derives a three dimensional (3D) wind vector from the  
187 differences of travel path between the three pairs. We inferred updraft velocity from uSonic measurements and could  
188 compare it to Doppler wind LiDAR (light detection and ranging) data, which provides 3D profiles starting from around  
189 150 m a.g.l. up to 10 km and beyond. The wind LiDAR (WindCube 200, Leosphere, Paris, France; property of  
190 AWIPEV) projects a laser beam (vertically for vertical velocity) and measures the Doppler shift between the reference  
191 and the backscattered radiation, enabling it to estimate the wind component along the beam propagation direction.  
192 Detailed information on the principle of operation as well as recent improvements of the Doppler wind LiDAR can be  
193 found in Liu et al. (2019). An overview of the system and the long-term wind pattern over Ny-Ålesund can be found  
194 in Graßl et al. (2022). The wind LiDAR was located on the roof of the Atmospheric Observatory of Ny-Ålesund, at an  
195 altitude close to sea level and around two kilometers in horizontal distance from Zeppelin (Beck et al., 2017; 2018).  
196 A meteorological station located on the roof the Zeppelin station provided data of wind speed and direction,  
197 temperature and pressure.

198 **2.2.4 Cloud droplet concentration**

199 Cloud particle concentrations were sampled with the HOLographic cloud Imager for Microscopic Objects (HOLIMO;  
200 Beck et al., 2017; Ramelli et al., 2020). HOLIMO can image an ensemble of cloud droplets (with diameter above 6  
201  $\mu\text{m}$ ) in a three dimensional sample volume of about 15  $\text{cm}^3$ . A convolutional neural network trained and fine-tuned on  
202 cloud particles from holographic imagers is used to identify the cloud droplets from artifacts and ice crystals  
203 (Touloupas et al., 2020). The holographic imager was attached below the tethered balloon system HoloBalloon  
204 (Ramelli et al., 2020; Pasquier et al., 2022).

205 **3 Data analysis and methods**

206 **3.1 Particle number size distribution, composition and aerosol hygroscopicity**

207 Based on the comparison between both DMPSs given in Sect. 4.1, we utilized data from both DMPSs in the analysis  
208 of this study, so that gaps in DMPS\_1 data are filled with data from DMPS\_2. All figures displaying aerosol number  
209 concentrations thus include data from both DMPSs.

210 Organic mass concentration was provided by the ACSM, while organic carbon concentration was measured by a high-  
211 volume sampler. The organic carbon concentration given by the filter analysis from this instrument was multiplied by  
212 a factor of 2.2 to obtain an estimation of the organic mass concentration, following the recommendations of Turpin  
213 and Lim (2001).

214 Chloride and sodium are assumed to be the only compounds predominantly present in the coarse mode, whereas the  
215 two DMPSs only measured in the submicron range, and the ToF-ACSM does not measure sea salt. This is an issue  
216 because the inputs of the cloud droplet parameterization should consider the size distribution and hygroscopicity of the



217 same aerosol population. For that reason, chloride and sodium were not included in the calculation of aerosol  
218 hygroscopicity. However, we know that these compounds can contribute to the fine mode and increase submicron  
219 hygroscopicity at Zeppelin, mostly in winter, as shown by Zieger et al., (2010) and Adachi et al. (2022). To estimate  
220 the potential effect of these compounds on our droplet formation results, we performed a sensitivity study, detailed in  
221 Sect. 4.3.

222 Both the ACSM and the filterpack allow for the retrieval of inorganic nitrate, sulphate and ammonium mass  
223 concentration. Volume fractions of neutral salts and their hygroscopicity parameters are used as inputs to the volumetric  
224 mixing rule required to calculate the total hygroscopicity of the aerosol. For both datasets, we used the simplified ion  
225 pairing scheme detailed in Gysel et al. (2007) to calculate the concentration of neutral salts from that of ions, using  
226 daily averaged data. From there, the total hygroscopicity parameter  $\kappa$  was introduced by Petters and Kreidenweis  
227 (2007) to describe aerosol hygroscopicity based on a semi-empirical parameterization of the Raoult effect. Knowing  
228 the hygroscopicity value of each neutral compound - we utilized values listed in Petters and Kreidenweis (2007),  
229 Carrico et al. (2010) and Zieger et al. (2017) - the mass-mixing rule enables to estimate the overall aerosol  
230 hygroscopicity. We utilized filterpack-derived hygroscopicity values as input to the cloud droplet parameterization  
231 described in the next section because the filterpack shows less data gaps than the ACSM over the duration of the  
232 NASCENT campaign. ACSM-derived hygroscopicity is thus only used as a validation of the filterpack-derived  
233 hygroscopicity values retrieved (see the comparison of both in Fig. S3).

### 234 3.2 Cloud droplet number concentration and cloud supersaturation

235 Knowledge of particle number size distribution, overall hygroscopicity parameter  $\kappa$  as well as air temperature and  
236 pressure allow for the determination of the potential cloud droplet number concentration,  $N_d$ , the maximum available  
237 cloud supersaturation,  $S_{max}$ , and the minimum diameter required for an aerosol particle to activate to a cloud droplet,  
238  $D_{act}$ , using a cloud droplet formation parameterization. Note that the term "potential" is used to describe these outputs  
239 because the parameterization results include periods when no clouds were effectively present at Zeppelin. Based on  
240 cloud parcel theory, this parameterization was initially developed by Nenes and Seinfeld (2003) and improved with  
241 new implementations successively by Fountoukis and Nenes (2005), Barahona et al. (2010) and Morales Betancourt  
242 and Nenes (2014). Results of  $N_d$  and  $S_{max}$  are then constrained by updraft velocity measurements, here given by a  
243 uSonic and a wind LiDAR (Sect. 2.2.3). The activation parameterization is based on cloud parcel theory and solves the  
244 equations that describe droplet formation in an ascending air parcel containing aerosols and water vapor, specifically  
245 at the point where supersaturation becomes equal to  $S_{max}$ ;  $N_d$  is then equal to the number of CCN with critical  
246 supersaturation less than  $S_{max}$ . The parameterization uses as inputs the observed pressure and the temperature, the  
247 aerosol size distribution data, the hygroscopicity parameter  $\kappa$  and the updraft velocities.

248 We extracted wind LiDAR data corresponding to the updraft velocity at 500 m above ground level to make them  
249 comparable to uSonic data from Zeppelin station. We noticed surprisingly high values of vertical velocity measured  
250 by the uSonic during northern wind conditions (Fig. S1), which we attribute to the presence of winds orographically  
251 lifted by the Zeppelin mountain. Based on Fig. S1, we decided to discard uSonic data when the wind direction was  
252 between 335 and 15 degrees, so that any droplet calculation made is more representative of regional conditions than  
253 specific conditions at Zeppelin during strong orographically driven updrafts.





254 The high resolution of wind LiDAR and ultrasonic anemometer data reveals the highly variable nature of vertical  
255 velocity; to calculate droplet numbers relevant for the average cloud, we use the probabilistic approach detailed in  
256 Georgakaki et al. (2021): wind LiDAR data are grouped by hour and each block of 1 hour data is fitted to half-Gaussian  
257 probability density functions (PDFs) with a zero mean and a standard deviation  $\sigma_w$ . The cloud droplet formation  
258 parameterization is then applied for a characteristic velocity,  $w^* = 0.79 \sigma_w$ , as this provides the average droplet number  
259 over the distribution of positive velocities in the domain. A comparison of the results of this analysis derived from the  
260 uSonic and the wind LiDAR are shown in Fig. S2. Several studies performed using this approach gave successful  
261 droplet closures for  $N_d$  and  $S_{max}$  in various types of clouds (e.g., Fountoukis et al., 2007; Kacarab et al., 2020;  
262 Georgakaki et al., 2021). Note that this approach is not valid for boundary layers that undergo deep convection but  
263 only for low vertical velocities typical of boundary layer ascent and descent over a diurnal cycle, which is the case for  
264 Zeppelin (Di Liberto et al., 2012; Collaud Coen et al., 2018).

## 265 **4 Results and discussion**

### 266 **4.1 Particle number concentration and size distribution**

267 Fig. 1a presents  $N_{aer}$  time series, with values that show a minimum in October 2019 ( $20 - 60 \text{ cm}^{-3}$ ) followed by a  
268 relatively constant increase until an upper plateau ( $100 - 1000 \text{ cm}^{-3}$ ) reached between May and August 2020. A sharp  
269 decrease in  $N_{aer}$  is then observed towards the October minimum. Although with a shift of a month for the high  
270 concentration plateau, these measurements are in good agreement with the annual cycle of particle concentration  
271 reported by Tunved et al. (2013) averaged over ten years from 2000 to 2010 at Zeppelin. Aerosol levels measured at  
272 Zeppelin during the NASCENT campaign can thus be considered typical for this site. Overlapping periods of both  
273 DMPSs allow for a comparison of  $N_{aer}$  (see Fig. 1b) and confirm the strong correlation between both instruments.

### 274 **4.2 Aerosol hygroscopicity parameter $\kappa$**

275 The time series of  $\kappa$  values derived from both the filterpack and the ACSM data is shown in Fig. S3a. Both instruments,  
276 despite being based on techniques with a different aerosol size cut-off ( $\text{PM}_{2.5}$  for the ACSM and  $\text{PM}_{10}$  for the  
277 filterpack), generally provide  $\kappa$  values that agree to within 50% for the majority of data points (Fig. S3b). The mean  
278 hygroscopicity parameter  $\kappa$  value over the whole campaign was 0.40 when derived from the ACSM and 0.32 from the  
279 filterpack. Temporal trend shows a relatively constant  $\kappa$  value around 0.3 in fall, winter and spring, but a slightly lower  
280 value in summer, dropping to approximately 0.2, although rather variable.

281 A small number of field campaigns at Zeppelin investigated aerosol hygroscopicity. In summer 2008, Zábori  
282 et al., (2015) utilized both bulk chemical composition and size-resolved CCN measurements, retrieving  $\kappa$  values of  
283 respectively 0.5 and 0.3-0.4, slightly higher than our results. Zieger et al. (2010) measured wet and dry aerosol  
284 scattering from July to October 2008 using humidified and dry nephelometers. Using Mie theory, they were able to  
285 retrieve the hygroscopicity parameter  $\kappa$  and found a mean value of 0.57. This is also higher than the values we report  
286 in Fig. S3a, but the techniques used and the seasons studied are different. The median  $\kappa$  value of 0.23, retrieved by  
287 Jung et al. (2018), based on 5 years of CCN-scanning mobility particle sizer (SMPS) measurements, however agree





288 with our results. Year-round hygroscopic growth measurements by Rastak et al., (2014) led to the conclusion that the  
289 influence of hygroscopic growth on the direct radiative effect was higher in summer than during the Arctic Haze period.  
290 The hygroscopicity parameter has been constrained also in other locations in the Arctic, all of them combining a CCN  
291 counter and an instrument measuring particle number size distribution, either an ultra-high sensitivity aerosol  
292 spectrometer (UHSAS), a SMPS or a DMPS to provide input data for  $\kappa$ -Köhler theory calculations. Moore et al. (2011)  
293 and Herenz et al. (2018) both characterized springtime Arctic aerosol. The former reported values around 0.4 for  
294 background air masses and slightly below 0.6 for Arctic boundary layer in aircrafts flying over northern Alaska (USA);  
295 the latter retrieved a  $\kappa$  value of 0.23 at a station located in the Inuvik region in Canada. Martin et al. (2011) and Latham  
296 et al. (2013) ran measurements in the summer season and found similar values (average of 0.33 and 0.32, respectively),  
297 on an icebreaker on its way from Svalbard to the proximity of the North pole and on aircrafts flights between Alberta  
298 (Canada) and Greenland. Also in summer, but at a ground-based station in northern Sweden (68° North), Kammermann  
299 et al. (2010) retrieved lower  $\kappa$  values, between 0.07 and 0.21, but the close presence of the Stordalen mire, known to  
300 emit organic precursors, could cause a local reduction in aerosol hygroscopicity. At the Villum station in northeastern  
301 Greenland, Massling et al. (2022) reported  $\kappa$  values very close to the present study using CCN-SMPS measurements:  
302 0.28-0.35 in spring, and 0.23-0.35 in summer.

### 303 **4.3 Potential cloud supersaturation, droplet number concentration and activation diameter**

304 The cloud droplet formation parameterization outputs  $S_{\max}$ ,  $N_d$  and  $D_{\text{act}}$  are displayed as a time series in Fig. 2, together  
305 with the measured values of  $\sigma_w$ , which are used to constrain the parameterization. During periods of rain (noted in Fig.  
306 1a), the aerosol load was strongly reduced, directly implying sharp decreases in  $N_d$  and  $D_{\text{act}}$  which impact the other  
307 parameters. As expected,  $S_{\max}$  and  $\sigma_w$  covaried during the whole year, since turbulence and vertical velocity are primary  
308 drivers of cloud supersaturation generation. Values of  $S_{\max}$  were highest in fall, centered around 1% and reaching up  
309 to 4% (Fig. 1b). Except for a drop in early August,  $S_{\max}$  values ranged between around 0.5% and 1.5% in the second  
310 half of spring and in summer.

311 Together with Bougiatioti et al. (2020), Kacarab et al. (2020) examined the conditions for which cloud formation is  
312 insensitive to any increase in  $N_{\text{aer}}$  (i.e., updraft-limited regime) and found that it corresponds to when  $S_{\max}$  is below  
313 0.1%. Subsequent studies (e.g., Georgakaki et al., 2021) also supported this criterion, which is the one we decided to  
314 use here as well. Fig. 2b indicates that such conditions only occurred over short periods in winter and during the first  
315 half of spring. This shows that updraft velocity-limited conditions can be found, although very rarely, in the Svalbard  
316 archipelago when aerosol concentrations approach the Arctic haze maximum in winter and early spring (Fig. 2b). This  
317 is an important result, because when these conditions occur, cloud formation is not linearly influenced by these large  
318 aerosol loads, but only until a certain threshold, which will be discussed in the following.

319  $N_d$ , however, is not clearly linked to  $S_{\max}$ , but follows the trend of  $N_{\text{aer}}$  shown in Fig. 1a (this is confirmed by the  
320 scatterplots in Fig. 3) because a higher number of aerosol particles goes with a higher number of CCN on which water  
321 vapour can condense, as shown at Zeppelin by Jung et al. (2018). On the other hand, higher  $N_{\text{aer}}$  also results in a more  
322 intense competition for water vapour, leading to a decrease in  $S_{\max}$ , which in turn tends to limit  $N_d$ . Measuring the  
323 annual cycle of cloud residual number concentration at the same site from November 2015 to February 2018 using a  
324 ground-based counterflow virtual impactor (GCVI) inlet, Karlsson et al. (2021) reported a similarly high and variable



325 plateau between April and August as well as a minimum in fall. They however reported very low concentrations in  
326 January in February, followed by an extremely sharp increase from March to April. Our results show a steadier increase  
327 over the whole winter, in agreement with the increase in  $N_{\text{aer}}$  (Fig. 1a).

328 Clear seasonal variations in  $D_{\text{act}}$  can also be seen: the pristine-like conditions in fall and early winter associated with  
329 high cloud supersaturations led to low values of  $D_{\text{act}}$ , with frequent occurrences below 20 nm (Fig. 2d). These are even  
330 lower diameters than the values reported by Koike et al. (2019) – minimum  $D_{\text{act}}$  around 30 to 50 nm – using air parcel  
331 model calculations. Together with relatively high  $S_{\text{max}}$  at this period of the year, the very low aerosol concentrations,  
332 mainly concentrated in the accumulation mode (Tunved et al., 2013), leads to their efficient activation to cloud droplets,  
333 in agreement with previous results from Siegel et al. (2022). Although anthropogenic pollution transported from lower  
334 latitudes during the Arctic haze period (late winter and spring; Rahn, 1981) controls the CCN and droplet population,  
335 only a fraction of it was activated to cloud droplets, as larger  $D_{\text{act}}$  values, centered around 50-100 nm, were in the range  
336 of accumulation mode particles typically linked to this type of atmospheric transport. Such  $D_{\text{act}}$  values persisted over  
337 the summer with a particularly high peak between 100 and 200 nm at the beginning of August. Similarly, the dominant  
338 Aitken mode, originating from the intense new particle formation activity, likely stayed to a very large extent in the  
339 interstitial (unactivated) phase.

340 With a view to consistency with data from the DMPSs, the cloud droplet parameterization outputs shown in  
341 Fig. 2 are based on hygroscopicity calculations that do not include sodium and chloride, under the assumption that  
342 submicron aerosol particles do not contain these compounds. According to Adachi et al. (2022), this assumption may  
343 not be fully correct, as particles of 1  $\mu\text{m}$  in winter are found to be composed of 50% by mass of sea salt, with a  
344 decreasing proportion with decreasing particle diameter. To address any effects of sea salt on droplet formation, we  
345 performed a sensitivity analysis assuming the extreme case for which half of the measured aerosol mass was sea salt  
346 and repeated the analysis detailed above. Using a  $\kappa$  value of 1.1 for sea salt, as suggested by Zieger et al. (2017), the  
347 overall hygroscopicity shifted from values of 0.2-0.3 (see Fig. S3) to around 0.7. Fig. S4 shows the seasonal percent  
348 change such an increase in aerosol hygroscopicity has on  $N_{\text{d}}$ ,  $S_{\text{max}}$  and  $D_{\text{act}}$ . The two former parameters are very slightly  
349 affected in fall, winter and spring (up to  $\sim 5\%$  for  $N_{\text{d}}$ ). In summer they undergo a 20% change, but this is the season  
350 when the effective sea salt fraction is the lowest, as shown by Adachi et al. (2022), making such an effective change  
351 particularly unlikely. Values of  $D_{\text{act}}$  are more affected, although moderately with a reduction of around 30% regardless  
352 of the season. Overall, this sensitivity analysis shows that aerosol hygroscopicity effects from sea salt may have a  
353 second order influence on the cloud droplet parameterization outputs, and thus, would not significantly affect the results  
354 and conclusions based on the base case hygroscopicity value.

#### 355 4.4 Limiting droplet number concentration

356 During updraft-limited cloud formation conditions, values of  $N_{\text{d}}$  reach an upper limit, independent on  $N_{\text{aer}}$ , which  
357 Kacarab et al. (2020) suggested to name the limiting droplet number concentration,  $N_{\text{d}}^{\text{lim}}$ . This upper limit can be  
358 visualized as a plateau for which  $S_{\text{max}}$  drops below 0.1% when plotting  $N_{\text{d}}$  as a function of  $N_{\text{aer}}$ . This is shown in Fig.  
359 3, where as a sensitivity analysis, we prescribed three different  $\sigma_{\text{w}}$  values, 0.1, 0.2 and 0.3  $\text{m s}^{-1}$  for running the cloud  
360 droplet parameterization. Note that the three values of  $\sigma_{\text{w}}$  chosen here are representative of the stratiform cloud  
361 conditions typically prevailing in the Arctic. Based on the results in Sect. 4.3, updraft-limited conditions were observed



362 in winter and early spring. Extracting mean plateau values corresponding to these seasons from Fig. 3, we retrieved  
363  $N_d^{\text{lim}}$  values of  $173 \text{ cm}^{-3}$  for winter and  $128 \text{ cm}^{-3}$  for spring, when an updraft velocity  $\sigma_w = 0.1 \text{ m s}^{-1}$  is prescribed. These  
364 results are in good agreement with the 2 years averaged peak concentration of cloud residuals measured by Karlsson  
365 et al. (2021) for April and May. This implies that when updraft velocity was low at the Zeppelin station in winter and  
366 early spring, only the fraction of the aerosol number concentration corresponding to these seasonal plateau values  
367 formed cloud droplets; any surplus of aerosol (very likely during Arctic haze conditions) remained in the interstitial  
368 phase.

369 Adding up to the different regimes of cloud formation distinguished in Sect 4.3., the  $N_d^{\text{lim}}$  plateau is almost never  
370 reached in fall and in summer. Short drops in  $S_{\text{max}}$  below 0.1% occurred, e.g. at the beginning of December and August  
371 as shown in Fig. S1b, but over too short periods for them to be associated as updraft velocity-limited conditions. For  
372 that reason, we do not consider the summer  $S_{\text{max}}$  values below 0.1% in Fig. 3 as a relevant  $N_d^{\text{lim}}$  plateau value.

373 In addition, it is worth noting that when applying the same analysis with an assumption on  $\sigma_w$  of  $0.2$  or  $0.3 \text{ m s}^{-1}$  (middle  
374 and right panels in Fig. 3) and even higher (not shown), the 0.1%  $S_{\text{max}}$  threshold is not reached at all, neither in winter  
375 nor in spring, indicating that vertical velocity-limited conditions cannot be found if the turbulence of the boundary  
376 layer is not extremely low.

377 Observing the shape of the plots displayed in Fig. 3 also provides information on the efficiency of cloud droplet  
378 formation and corroborates the results discussed above. The high  $S_{\text{max}}$  and corresponding low  $D_{\text{act}}$  in fall and winter  
379 are associated to the droplet activation of the whole aerosol population, leading  $N_d^{\text{lim}}$  to match  $N_{\text{aer}}$ ; these two  
380 parameters are thus represented in a scatterplot as a narrow band close to the 1:1 relationship. On the contrary, the  
381 scatterplot for the summer season shows a much larger spread with an offset from the 1:1 line, in agreement with a  
382 large proportion of Aitken mode aerosol particles that did not activate to cloud droplets. Interestingly, the sharp  
383 transition between these two activation behaviours, also observed by Engvall et al. (2008) and which we have shown  
384 to occur in the middle of spring (Fig. 2a-b-c), results in a scatterplot where both staggered and matching  $N_d - N_{\text{aer}}$   
385 relationships can be observed.

386 Extracting the plateau values of  $N_d^{\text{lim}}$  from Fig. 3, we investigate their relationship with  $\sigma_w$  in different types of clouds  
387 located in various geographic locations using previous studies in which the same probabilistic analysis was performed  
388 (Fig. 4). Kacarab et al. (2020) measured from an aircraft in summer in the marine boundary layer over the southeastern  
389 Atlantic, a region that can be strongly influenced by biomass burning fires from the African continent. They retrieved  
390 values of  $\sigma_w$  between  $0.30$  (relatively clean air mass) and  $0.56 \text{ m s}^{-1}$  (more polluted) for which  $N_d^{\text{lim}}$  was reached.  
391 Georgakaki et al. (2021) also reported  $\sigma_w$  values as high as  $0.5 \text{ m s}^{-1}$  in two mid-altitude stations located in the Swiss  
392 Alps in central Europe. The fact that they had winter measurements allowed them to reach values as low as  $0.1 \text{ m s}^{-1}$ ,  
393 making their results directly comparable to those shown here. They could link this value of  $\sigma_w$  to an  $N_d^{\text{lim}}$  plateau of  
394  $108.1 \text{ cm}^{-3}$ . At the other side of the spectrum, Bougiatioti et al. (2020) reached an  $N_d^{\text{lim}}$  plateau for  $\sigma_w$  values as high  
395  $1.2 \text{ m s}^{-1}$  thanks to late spring and summer flights in the boundary layer over the southeastern United States. They  
396 proposed the following linear correlation between  $N_d^{\text{lim}} [\text{cm}^{-3}]$  and  $\sigma_w [\text{m s}^{-1}]$ :  $N_d^{\text{lim}} = 1033.9 \sigma_w + 112.28$  ( $R^2 = 0.92$ ).  
397 Georgakaki et al. (2021) updated this relationship, including the results from Kacarab et al. (2020) and their own:  $N_d^{\text{lim}}$   
398  $= 1137.9 \sigma_w - 17.1$ , and proved very strong agreement between all reported data ( $R^2 = 0.94$ ). The two additions from  
399 the present study, associated to winter and spring plateau values for  $\sigma_w = 0.1 \text{ m s}^{-1}$ , also agree well with these previous



400 results, although they were retrieved in a very different environment, relatively clean with clouds mainly originating  
401 from maritime air masses and uplifted in mountainous terrain. This provides another confirmation of the robustness of  
402 the empirically demonstrated  $\sigma_w - N_d^{\text{lim}}$  relationship regardless of the environment, type of clouds and aerosol sources.

#### 403 **4.5 Droplet closure**

404  $N_d$  is one of the outputs provided by the cloud droplet formation parameterization utilized in the present study (see  
405 Fig. 2c). The availability of instruments measuring this parameter facilitates the validation of the cloud droplet  
406 parameterization by comparing in situ data with the parameterization output. This was achieved several times in past  
407 studies through successful droplet closures (e.g. Fountoukis et al., 2007; Kacarab et al., 2020), and can also be  
408 performed here using measurements from the HOLIMO taken on 9 HoloBalloon flights during the NASCENT  
409 campaign (Fig. 5; see Pasquier et al. (2022a) for detailed descriptions of the atmospheric conditions during the flights).  
410 The closure appears successful for  $N_d > 8\text{-}10 \text{ cm}^{-3}$ , thereby validating the use of the cloud droplet formation  
411 parameterization in the Arctic environment. Values of  $N_d$  below  $8\text{-}10 \text{ cm}^{-3}$  approach the minimum threshold  
412 concentration for which a cloud can still be defined as such, potentially including periods when droplet nucleation is  
413 not effectively occurring or has been followed by out-of-cloud scavenging.

414 Mixed-phase clouds tend to rapidly glaciate (i.e., convert to pure ice clouds) due to the Wegener-Bergeron-Findeisen  
415 (WBF) process or riming (Korolev et al., 2017), which can effectively transfer mass from the liquid to the ice phase.  
416 Nevertheless, Fig. 5 provides evidence that even at high degrees of glaciation (as high as 90%), cloud parcel activation  
417 theory can predict  $N_d$  accurately. This implies that the cloud liquid water content is not significantly involved in the  
418 glaciation process. Instead, secondary ice production (SIP) through ice-ice collisions or droplet-shattering may justify  
419 high glaciation fraction without depleting small cloud droplets (Field et al., 2017; Korolev and Leisner, 2020) over the  
420 duration of the HoloBalloon flights, and most probably over spring and fall. SIP through rime-splintering is unlikely  
421 as it would have reduced the available  $N_d$ . This hypothesis is in line with the findings of Pasquier et al. (2022a), where  
422 the effect of SIP was inferred in about 40% of the in-cloud measurements.

423 Previous observations (Borys et al., 2003; Lance et al., 2011; Norgren et al., 2018) reported that large aerosol loadings  
424 could hamper the efficiency of riming in mixed-phase clouds. Here we show that even in the very pristine conditions  
425 during winter and spring, the amount of riming does not seem to affect the droplet number concentrations significantly  
426 from what is expected from warm cloud activation theory.

#### 427 **5 Summary and Conclusions**

428 Measurements performed over a whole year at the Zeppelin station in the Svalbard archipelago, in the framework of  
429 the NASCENT campaign, served as inputs for a semi-empirical parameterization whose use was validated through a  
430 droplet closure. This led to unravel different characteristics of cloud droplet formation in the Arctic environment:

431 • Several studies focusing on the factors limiting cloud droplet formation were recently published and revealed precious  
432 information on boundary layer clouds with high updraft velocities such as cumulus and stratocumulus clouds, but also  
433 in alpine mixed-phase clouds that can form in more stable air dynamics. The current study demonstrates that updraft-



434 velocity cloud formation can also occur in a relatively unpolluted environment with weak convection of maritime air  
435 masses such as the Arctic, during winter and early spring.

436 • During the fall and early winter period, the high cloud supersaturations encountered allow to efficiently activate to  
437 cloud droplets the vast majority of the aerosol population. By late winter and spring (Arctic Haze period), accumulation  
438 mode particles transported over long-range pathways contribute to cloud formation, although cloud supersaturations,  
439 and hence activation diameters, are highly variable. Interestingly, the onset of intense new particle formation in summer  
440 coincides with an increase in activation diameters. Newly formed and dominant Aitken mode particles thus barely  
441 participate in cloud formation before they grow to larger sizes over the course of summer and fall.

442 • The recent interest in understanding the response of the limiting droplet number concentration to variations in updraft  
443 velocity has led to describe a relationship between these two parameters that showed to be strikingly similar in very  
444 diverse environments, intensities of atmospheric convection and types of clouds. We showed that, as unpolluted and  
445 weakly dynamic as it is, the Arctic environment is no exception. This is an important step towards the confirmation of  
446 the universality of the  $N_d^{\text{lim}} - \sigma_w$  relationship.

447 • Insights into the mechanisms of secondary ice production in the Arctic spring and fall could be extracted from our  
448 droplet closure. They suggest that riming was not taking place in any significant amount, leaving room for ice-ice  
449 collisions and droplet shattering as the main mechanisms of glaciation, in addition to primary ice production. This also  
450 means that warm cloud activation theory, such as described by well-established activation parameterizations (e.g.,  
451 Morales and Nenes, 2014) are appropriate for application in mixed-phase cloud simulations.

#### 452 **Author contribution**

453 GM and AN conceived and designed the study. GM, AN and PG developed the data analysis methods, AN developed  
454 the droplet calculation codes and performed the simulations with GM. GM authored the manuscript with input from  
455 AN and PG. CR provided the wind lidar data. CL and WA provided the chemical composition data (filterpack and  
456 ToF-ACSM) from Zeppelin. JW helped with ground-based aerosol and the balloon-borne cloud measurements, and  
457 contributed to the discussion and interpretation. ROD helped with the balloon-borne and conducted the mountaintop  
458 cloud measurements. All co-authors commented on the manuscript and provided feedback. RK, PZ and GF provided  
459 aerosol microphysical and meteorological data from Zeppelin station and contributed to the interpretation and  
460 manuscript editing and commenting.

#### 461 **Acknowledgements**

462 We would like to thank the Norwegian Polar Institute (NPI) for logistical support at Ny-Ålesund and Zeppelin, as well  
463 as every person involved in the planning, measurements and data analysis of the NASCENT campaign (a project  
464 initiated by the Stockholm University). This work is supported by the European Research Council, CoG-2016 project  
465 PyroTRACH (726165) funded by H2020-EU.1.1. – Excellent Science, and from the European Union Horizon 2020  
466 project FORCeS under grant agreement No 821205. We also acknowledge funding from the Swedish Environmental  
467 Protection Agency (Naturvårdsverket), the Knut and Alice Wallenberg Foundation (WAF project CLOUDFORM,



468 grant no. 2017.0165), the project ACAS (project no. 2016.0024), the funding agency FORMAS (IWCAA project no.  
469 2016-01427), the European Research Council (ERC) through Grant StG758005 and the EU/Norway Grants EEARO-  
470 NO-2019-0423/IceSafari, contract no. 31/2020, the Swedish Research Council (Vetenskapsrådet starting grant, project  
471 number 2018-05045) and the Swiss National Science Foundation (grant no. 200021\_175824). Funding for the OC/EC  
472 and ToF-ACSM measurements are provided by the Norwegian Ministry of Climate and Environment while the  
473 inorganic measurements from the filterpack are funded by the Norwegian Environment Agency.

474

475 The authors declare that they have no conflict of interest.

#### 476 **References**

477 Adachi, K., Tobo, Y., Koike, M., Freitas, G., Zieger, P., and Krejci, R.: Composition and mixing state of Arctic aerosol  
478 and cloud residual particles from long-term single-particle observations at Zeppelin Observatory, Svalbard,  
479 *Atmospheric Chemistry and Physics*, 22, 14421–14439, <https://doi.org/10.5194/acp-22-14421-2022>, 2022.

480 Barahona, D., West, R. E. L., Stier, P., Romakkaniemi, S., Kokkola, H., and Nenes, A.: Comprehensively accounting  
481 for the effect of giant CCN in cloud activation parameterizations, *Atmospheric Chemistry and Physics*, 10, 2467–2473,  
482 <https://doi.org/10.5194/acp-10-2467-2010>, 2010.

483 Beck, A., Henneberger, J., Schöpfer, S., Fugal, J., and Lohmann, U.: HoloGondel: in situ cloud observations on a cable  
484 car in the Swiss Alps using a holographic imager, *Atmospheric Measurement Techniques*, 10, 459–476,  
485 <https://doi.org/10.5194/amt-10-459-2017>, 2017.

486 Beck, A., Henneberger, J., Fugal, J. P., David, R. O., Lacher, L., and Lohmann, U.: Impact of surface and near-surface  
487 processes on ice crystal concentrations measured at mountain-top research stations, *Atmospheric Chemistry and  
488 Physics*, 18, 8909–8927, <https://doi.org/10.5194/acp-18-8909-2018>, 2018.

489 Borys, R. D., Lowenthal, D. H., Cohn, S. A., and Brown, W. O. J.: Mountaintop and radar measurements of  
490 anthropogenic aerosol effects on snow growth and snowfall rate, *Geophysical Research Letters*, 30,  
491 <https://doi.org/10.1029/2002GL016855>, 2003.

492 Bougiatioti, A., Nenes, A., Lin, J. J., Brock, C. A., de Gouw, J. A., Liao, J., Middlebrook, A. M., and Welti, A.: Drivers  
493 of cloud droplet number variability in the summertime in the southeastern United States, *Atmospheric Chemistry and  
494 Physics*, 20, 12163–12176, <https://doi.org/10.5194/acp-20-12163-2020>, 2020.

495 Breider, T. J., Mickley, L. J., Jacob, D. J., Ge, C., Wang, J., Payer Sulprizio, M., Croft, B., Ridley, D. A., McConnell,  
496 J. R., Sharma, S., Husain, L., Dutkiewicz, V. A., Eleftheriadis, K., Skov, H., and Hopke, P. K.: Multidecadal trends in  
497 aerosol radiative forcing over the Arctic: Contribution of changes in anthropogenic aerosol to Arctic warming since  
498 1980, *Journal of Geophysical Research: Atmospheres*, 122, 3573–3594, <https://doi.org/10.1002/2016JD025321>, 2017.  
499 Bulatovic, I., Igel, A. L., Leck, C., Heintzenberg, J., Riipinen, I., and Ekman, A. M. L.: The importance of Aitken mode  
500 aerosol particles for cloud sustenance in the summertime high Arctic – a simulation study supported by observational  
501 data, *Atmospheric Chemistry and Physics*, 21, 3871–3897, <https://doi.org/10.5194/acp-21-3871-2021>, 2021.





- 502 Carrico, C. M., Petters, M. D., Kreidenweis, S. M., Sullivan, A. P., McMeeking, G. R., Levin, E. J. T., Engling, G.,  
503 Malm, W. C., and Collett, J. L. J.: Water uptake and chemical composition of fresh aerosols generated in open burning  
504 of biomass, *Atmospheric Chemistry and Physics*, 10, 5165–5178, <https://doi.org/10.5194/acp-10-5165-2010>, 2010.
- 505 Cavalli, F., Viana, M., Yttri, K. E., Genberg, J., and Putaud, J.-P.: Toward a standardised thermal-optical protocol for  
506 measuring atmospheric organic and elemental carbon: the EUSAAR protocol, *Atmospheric Measurement Techniques*,  
507 3, 79–89, <https://doi.org/10.5194/amt-3-79-2010>, 2010.
- 508 Collaud Coen, M., Andrews, E., Aliaga, D., Andrade, M., Angelov, H., Bukowiecki, N., Ealo, M., Fialho, P., Flentje,  
509 H., Hallar, A. G., Hooda, R., Kalapov, I., Krejci, R., Lin, N.-H., Marinoni, A., Ming, J., Nguyen, N. A., Pandolfi, M.,  
510 Pont, V., Ries, L., Rodríguez, S., Schauer, G., Sellegri, K., Sharma, S., Sun, J., Tunved, P., Velasquez, P., and Ruffieux,  
511 D.: Identification of topographic features influencing aerosol observations at high altitude stations, *Atmospheric*  
512 *Chemistry and Physics*, 18, 12289–12313, <https://doi.org/10.5194/acp-18-12289-2018>, 2018.
- 513 Croft, B., Martin, R. V., Leaitch, W. R., Tunved, P., Breider, T. J., D’Andrea, S. D., and Pierce, J. R.: Processes  
514 controlling the annual cycle of Arctic aerosol number and size distributions, *Atmospheric Chemistry and Physics*, 16,  
515 3665–3682, <https://doi.org/10.5194/acp-16-3665-2016>, 2016.
- 516 Curry, J. A., Schramm, J. L., Rossow, W. B., and Randall, D.: Overview of Arctic Cloud and Radiation Characteristics,  
517 *Journal of Climate*, 9, 1731–1764, [https://doi.org/10.1175/1520-0442\(1996\)009<1731:OOACAR>2.0.CO;2](https://doi.org/10.1175/1520-0442(1996)009<1731:OOACAR>2.0.CO;2), 1996.
- 518 Dall’Osto, M., Beddows, D. C. S., Tunved, P., Krejci, R., Ström, J., Hansson, H.-C., Yoon, Y. J., Park, K.-T., Becagli,  
519 S., Udisti, R., Onasch, T., O’Dowd, C. D., Simó, R., and Harrison, R. M.: Arctic sea ice melt leads to atmospheric new  
520 particle formation, *Sci Rep*, 7, 3318, <https://doi.org/10.1038/s41598-017-03328-1>, 2017.
- 521 Di Liberto, L., Angelini, F., Pietroni, I., Cairo, F., Di Donfrancesco, G., Viola, A., Argentini, S., Fierli, F., Gobbi, G.,  
522 Maturilli, M., Neuber, R., and Snels, M.: Estimate of the Arctic Convective Boundary Layer Height from Lidar  
523 Observations: A Case Study, *Advances in Meteorology*, 2012, e851927, <https://doi.org/10.1155/2012/851927>, 2012.
- 524 Ebell, K., Nomokonova, T., Maturilli, M., and Ritter, C.: Radiative Effect of Clouds at Ny-Ålesund, Svalbard, as  
525 Inferred from Ground-Based Remote Sensing Observations, *Journal of Applied Meteorology and Climatology*, 59, 3–  
526 22, <https://doi.org/10.1175/JAMC-D-19-0080.1>, 2020.
- 527 Eirund, G. K., Possner, A., and Lohmann, U.: Response of Arctic mixed-phase clouds to aerosol perturbations under  
528 different surface forcings, *Atmospheric Chemistry and Physics*, 19, 9847–9864, [https://doi.org/10.5194/acp-19-9847-](https://doi.org/10.5194/acp-19-9847-2019)  
529 2019, 2019.
- 530 Engvall, A.-C., Krejci, R., Ström, J., Treffeisen, R., Scheele, R., Hermansen, O., and Paatero, J.: Changes in aerosol  
531 properties during spring-summer period in the Arctic troposphere, *Atmospheric Chemistry and Physics*, 8, 445–462,  
532 <https://doi.org/10.5194/acp-8-445-2008>, 2008.
- 533 Field, P. R., Lawson, R. P., Brown, P. R. A., Lloyd, G., Westbrook, C., Moisseev, D., Miltenberger, A., Nenes, A.,  
534 Blyth, A., Choularton, T., Connolly, P., Buehl, J., Crosier, J., Cui, Z., Dearden, C., DeMott, P., Flossmann, A.,  
535 Heymsfield, A., Huang, Y., Kalesse, H., Kanji, Z. A., Korolev, A., Kirchgassner, A., Lasher-Trapp, S., Leisner, T.,  
536 McFarquhar, G., Phillips, V., Stith, J., and Sullivan, S.: Secondary Ice Production: Current State of the Science and  
537 Recommendations for the Future, *Meteorological Monographs*, 58, 7.1-7.20,  
538 <https://doi.org/10.1175/AMSMONOGRAPHS-D-16-0014.1>, 2017.



- 539 Fountoukis, C. and Nenes, A.: Continued development of a cloud droplet formation parameterization for global climate  
540 models, *Journal of Geophysical Research: Atmospheres*, 110, <https://doi.org/10.1029/2004JD005591>, 2005.
- 541 Fountoukis, C., Nenes, A., Meskhidze, N., Bahreini, R., Conant, W. C., Jonsson, H., Murphy, S., Sorooshian, A.,  
542 Varutbangkul, V., Brechtel, F., Flagan, R. C., and Seinfeld, J. H.: Aerosol–cloud drop concentration closure for clouds  
543 sampled during the International Consortium for Atmospheric Research on Transport and Transformation 2004  
544 campaign, *Journal of Geophysical Research: Atmospheres*, 112, <https://doi.org/10.1029/2006JD007272>, 2007.
- 545 Freud, E., Krejci, R., Tunved, P., Leaitch, R., Nguyen, Q. T., Massling, A., Skov, H., and Barrie, L.: Pan-Arctic aerosol  
546 number size distributions: seasonality and transport patterns, *Atmospheric Chemistry and Physics*, 17, 8101–8128,  
547 <https://doi.org/10.5194/acp-17-8101-2017>, 2017.
- 548 Fröhlich, R., Cubison, M. J., Slowik, J. G., Bukowiecki, N., Prévôt, A. S. H., Baltensperger, U., Schneider, J., Kimmel,  
549 J. R., Gonin, M., Rohner, U., Worsnop, D. R., and Jayne, J. T.: The ToF-ACSM: a portable aerosol chemical speciation  
550 monitor with TOFMS detection, *Atmospheric Measurement Techniques*, 6, 3225–3241, <https://doi.org/10.5194/amt-6-3225-2013>, 2013.
- 552 Garrett, T. J., Zhao, C., Dong, X., Mace, G. G., and Hobbs, P. V.: Effects of varying aerosol regimes on low-level  
553 Arctic stratus, *Geophysical Research Letters*, 31, <https://doi.org/10.1029/2004GL019928>, 2004.
- 554 Georgakaki, P., Bougiatioti, A., Wieder, J., Mignani, C., Ramelli, F., Kanji, Z. A., Henneberger, J., Hervo, M., Berne,  
555 A., Lohmann, U., and Nenes, A.: On the drivers of droplet variability in alpine mixed-phase clouds, *Atmospheric  
556 Chemistry and Physics*, 21, 10993–11012, <https://doi.org/10.5194/acp-21-10993-2021>, 2021.
- 557 Gramlich, Y., Siegel, K., Haslett, S. L., Freitas, G., Krejci, R., Zieger, P., and Mohr, C.: Revealing the chemical  
558 characteristics of Arctic low-level cloud residuals &ndash; in situ observations from a mountain site, *EGUsphere*, 1–  
559 29, <https://doi.org/10.5194/egusphere-2022-1395>, 2022.
- 560 Graßl, S., Ritter, C., and Schulz, A.: The Nature of the Ny-Ålesund Wind Field Analysed by High-Resolution  
561 Windlidar Data, *Remote Sensing*, 14, 3771, <https://doi.org/10.3390/rs14153771>, 2022.
- 562 Gysel, M., Crosier, J., Topping, D. O., Whitehead, J. D., Bower, K. N., Cubison, M. J., Williams, P. I., Flynn, M. J.,  
563 Mcfiggans, G. B., and Coe, H.: Closure study between chemical composition and hygroscopic growth of aerosol  
564 particles during TORCH2, *Atmospheric Chemistry and Physics*, 7, 6131–6144, 2007.
- 565 Hammer, E., Bukowiecki, N., Luo, B. P., Lohmann, U., Marcolli, C., Weingartner, E., Baltensperger, U., and Hoyle,  
566 C. R.: Sensitivity estimations for cloud droplet formation in the vicinity of the high-alpine research station Jungfraujoch  
567 (3580 m a.s.l.), *Atmospheric Chemistry and Physics*, 15, 10309–10323, <https://doi.org/10.5194/acp-15-10309-2015>,  
568 2015.
- 569 Herenz, P., Wex, H., Henning, S., Kristensen, T. B., Rubach, F., Roth, A., Borrmann, S., Bozem, H., Schulz, H., and  
570 Stratmann, F.: Measurements of aerosol and CCN properties in the Mackenzie River delta (Canadian Arctic) during  
571 spring–summer transition in May 2014, *Atmospheric Chemistry and Physics*, 18, 4477–4496,  
572 <https://doi.org/10.5194/acp-18-4477-2018>, 2018.
- 573 Hoyle, C. R., Webster, C. S., Rieder, H. E., Nenes, A., Hammer, E., Herrmann, E., Gysel, M., Bukowiecki, N.,  
574 Weingartner, E., Steinbacher, M., and Baltensperger, U.: Chemical and physical influences on aerosol activation in  
575 liquid clouds: a study based on observations from the Jungfraujoch, Switzerland, *Atmospheric Chemistry and Physics*,  
576 16, 4043–4061, <https://doi.org/10.5194/acp-16-4043-2016>, 2016.



577 Intrieri, J. M., Fairall, C. W., Shupe, M. D., Persson, P. O. G., Andreas, E. L., Guest, P. S., and Moritz, R. E.: An  
578 annual cycle of Arctic surface cloud forcing at SHEBA, *Journal of Geophysical Research: Oceans*, 107, SHE 13-1-  
579 SHE 13-14, <https://doi.org/10.1029/2000JC000439>, 2002.

580 Jensen, J. B. and Charlson, R. J.: On the efficiency of nucleation scavenging, *Tellus B: Chemical and Physical*  
581 *Meteorology*, 36, 367–375, <https://doi.org/10.3402/tellusb.v36i5.14917>, 1984.

582 Jung, C. H., Yoon, Y. J., Kang, H. J., Gim, Y., Lee, B. Y., Ström, J., Krejci, R., and Tunved, P.: The seasonal  
583 characteristics of cloud condensation nuclei (CCN) in the arctic lower troposphere, *Tellus B: Chemical and Physical*  
584 *Meteorology*, 70, 1–13, <https://doi.org/10.1080/16000889.2018.1513291>, 2018.

585 Kacarab, M., Thornhill, K. L., Dobracki, A., Howell, S. G., O'Brien, J. R., Freitag, S., Poellot, M. R., Wood, R.,  
586 Zuidema, P., Redemann, J., and Nenes, A.: Biomass burning aerosol as a modulator of the droplet number in the  
587 southeast Atlantic region, *Atmospheric Chemistry and Physics*, 20, 3029–3040, <https://doi.org/10.5194/acp-20-3029->  
588 2020, 2020.

589 Kammermann, L., Gysel, M., Weingartner, E., Herich, H., Cziczo, D. J., Holst, T., Svenningsson, B., Arneth, A., and  
590 Baltensperger, U.: Subarctic atmospheric aerosol composition: 3. Measured and modeled properties of cloud  
591 condensation nuclei, *Journal of Geophysical Research: Atmospheres*, 115, <https://doi.org/10.1029/2009JD012447>,  
592 2010.

593 Karlsson, L., Krejci, R., Koike, M., Ebell, K., and Zieger, P.: A long-term study of cloud residuals from low-level  
594 Arctic clouds, *Atmospheric Chemistry and Physics*, 21, 8933–8959, <https://doi.org/10.5194/acp-21-8933-2021>, 2021.

595 Koike, M., Ukita, J., Ström, J., Tunved, P., Shiobara, M., Vitale, V., Lupi, A., Baumgardner, D., Ritter, C., Hermansen,  
596 O., Yamada, K., and Pedersen, C. A.: Year-Round In Situ Measurements of Arctic Low-Level Clouds: Microphysical  
597 Properties and Their Relationships With Aerosols, *Journal of Geophysical Research: Atmospheres*, 124, 1798–1822,  
598 <https://doi.org/10.1029/2018JD029802>, 2019.

599 Korolev, A. and Leisner, T.: Review of experimental studies of secondary ice production, *Atmospheric Chemistry and*  
600 *Physics*, 20, 11767–11797, <https://doi.org/10.5194/acp-20-11767-2020>, 2020.

601 Korolev, A., McFarquhar, G., Field, P. R., Franklin, C., Lawson, P., Wang, Z., Williams, E., Abel, S. J., Axisa, D.,  
602 Borrmann, S., Crosier, J., Fugal, J., Krämer, M., Lohmann, U., Schlenczek, O., Schnaiter, M., and Wendisch, M.:  
603 Mixed-Phase Clouds: Progress and Challenges, *Meteorological Monographs*, 58, 5.1-5.50,  
604 <https://doi.org/10.1175/AMSMONOGRAPHS-D-17-0001.1>, 2017.

605 Lance, S., Shupe, M. D., Feingold, G., Brock, C. A., Cozic, J., Holloway, J. S., Moore, R. H., Nenes, A., Schwarz, J.  
606 P., Spackman, J. R., Froyd, K. D., Murphy, D. M., Brioude, J., Cooper, O. R., Stohl, A., and Burkhardt, J. F.: Cloud  
607 condensation nuclei as a modulator of ice processes in Arctic mixed-phase clouds, *Atmospheric Chemistry and Physics*,  
608 11, 8003–8015, <https://doi.org/10.5194/acp-11-8003-2011>, 2011.

609 Latham, T. L., Beyersdorf, A. J., Thornhill, K. L., Winstead, E. L., Cubison, M. J., Hecobian, A., Jimenez, J. L., Weber,  
610 R. J., Anderson, B. E., and Nenes, A.: Analysis of CCN activity of Arctic aerosol and Canadian biomass burning during  
611 summer 2008, *Atmospheric Chemistry and Physics*, 13, 2735–2756, <https://doi.org/10.5194/acp-13-2735-2013>, 2013.

612 Lawson, R. P., Stamnes, K., Stamnes, J., Zmarzly, P., Koskuliks, J., Roden, C., Mo, Q., Carrithers, M., and Bland, G.  
613 L.: Deployment of a Tethered-Balloon System for Microphysics and Radiative Measurements in Mixed-Phase Clouds



- 614 at Ny-Ålesund and South Pole, *Journal of Atmospheric and Oceanic Technology*, 28, 656–670,  
615 <https://doi.org/10.1175/2010JTECHA1439.1>, 2011.
- 616 Leaitch, W. R., Korolev, A., Aliabadi, A. A., Burkart, J., Willis, M. D., Abbatt, J. P. D., Bozem, H., Hoor, P., Köllner,  
617 F., Schneider, J., Herber, A., Konrad, C., and Brauner, R.: Effects of 20–100 nm particles on liquid clouds in the clean  
618 summertime Arctic, *Atmospheric Chemistry and Physics*, 16, 11107–11124, [https://doi.org/10.5194/acp-16-11107-](https://doi.org/10.5194/acp-16-11107-2016)  
619 2016, 2016.
- 620 Liu, Z., Barlow, J. F., Chan, P.-W., Fung, J. C. H., Li, Y., Ren, C., Mak, H. W. L., and Ng, E.: A Review of Progress  
621 and Applications of Pulsed Doppler Wind LiDARs, *Remote Sensing*, 11, 2522, <https://doi.org/10.3390/rs11212522>,  
622 2019.
- 623 Martin, M., Chang, R. Y.-W., Sierau, B., Sjogren, S., Swietlicki, E., Abbatt, J. P. D., Leck, C., and Lohmann, U.: Cloud  
624 condensation nuclei closure study on summer arctic aerosol, *Atmospheric Chemistry and Physics*, 11, 11335–11350,  
625 <https://doi.org/10.5194/acp-11-11335-2011>, 2011.
- 626 Massling, A., Lange, R., Pernov, J., Gosewinkel, U., Sørensen, L.-L., and Skov, H.: Measurement report: High Arctic  
627 aerosol hygroscopicity at sub- and supersaturated conditions during spring and summer, *Atmospheric Chemistry and*  
628 *Physics Discussions*, 1–30, <https://doi.org/10.5194/acp-2022-413>, 2022.
- 629 Maturilli, M., Herber, A., and König-Langlo, G.: Surface radiation climatology for Ny-Ålesund, Svalbard (78.9° N),  
630 basic observations for trend detection, *Theor Appl Climatol*, 120, 331–339, [https://doi.org/10.1007/s00704-014-1173-](https://doi.org/10.1007/s00704-014-1173-4)  
631 4, 2015.
- 632 Maturilli, M., Hanssen-Bauer, I., Neuber, R., Rex, M., and Edvardsen, K.: The Atmosphere Above Ny-Ålesund:  
633 Climate and Global Warming, Ozone and Surface UV Radiation, in: *The Ecosystem of Kongsfjorden, Svalbard*, edited  
634 by: Hop, H. and Wiencke, C., Springer International Publishing, Cham, 23–46, [https://doi.org/10.1007/978-3-319-](https://doi.org/10.1007/978-3-319-46425-1_2)  
635 46425-1\_2, 2019.
- 636 Mauritsen, T., Sedlar, J., Tjernström, M., Leck, C., Martin, M., Shupe, M., Sjogren, S., Sierau, B., Persson, P. O. G.,  
637 Brooks, I. M., and Swietlicki, E.: An Arctic CCN-limited cloud-aerosol regime, *Atmospheric Chemistry and Physics*,  
638 11, 165–173, <https://doi.org/10.5194/acp-11-165-2011>, 2011.
- 639 Mioche, G., Jourdan, O., Ceccaldi, M., and Delanoë, J.: Variability of mixed-phase clouds in the Arctic with a focus  
640 on the Svalbard region: a study based on spaceborne active remote sensing, *Atmospheric Chemistry and Physics*, 15,  
641 2445–2461, <https://doi.org/10.5194/acp-15-2445-2015>, 2015.
- 642 Moore, R. H., Bahreini, R., Brock, C. A., Froyd, K. D., Cozic, J., Holloway, J. S., Middlebrook, A. M., Murphy, D.  
643 M., and Nenes, A.: Hygroscopicity and composition of Alaskan Arctic CCN during April 2008, *Atmospheric*  
644 *Chemistry and Physics*, 11, 11807–11825, <https://doi.org/10.5194/acp-11-11807-2011>, 2011.
- 645 Morales Betancourt, R. and Nenes, A.: Droplet activation parameterization: the population-splitting concept revisited,  
646 *Geoscientific Model Development*, 7, 2345–2357, <https://doi.org/10.5194/gmd-7-2345-2014>, 2014.
- 647 Najafi, M. R., Zwiers, F. W., and Gillett, N. P.: Attribution of Arctic temperature change to greenhouse-gas and aerosol  
648 influences, *Nature Clim Change*, 5, 246–249, <https://doi.org/10.1038/nclimate2524>, 2015.
- 649 Nenes, A. and Seinfeld, J. H.: Parameterization of cloud droplet formation in global climate models, *Journal of*  
650 *Geophysical Research: Atmospheres*, 108, <https://doi.org/10.1029/2002JD002911>, 2003.



- 651 Nenes, A., Ghan, S., Abdul-Razzak, H., Chuang, P. Y., and Seinfeld, J. H.: Kinetic limitations on cloud droplet  
652 formation and impact on cloud albedo, *Tellus B: Chemical and Physical Meteorology*, 53, 133–149,  
653 <https://doi.org/10.3402/tellusb.v53i2.16569>, 2001.
- 654 Nomokonova, T., Ebell, K., Löhnert, U., Maturilli, M., Ritter, C., and O'Connor, E.: Statistics on clouds and their  
655 relation to thermodynamic conditions at Ny-Ålesund using ground-based sensor synergy, *Atmospheric Chemistry and  
656 Physics*, 19, 4105–4126, <https://doi.org/10.5194/acp-19-4105-2019>, 2019.
- 657 Norgren, M. S., de Boer, G., and Shupe, M. D.: Observed aerosol suppression of cloud ice in low-level Arctic mixed-  
658 phase clouds, *Atmospheric Chemistry and Physics*, 18, 13345–13361, <https://doi.org/10.5194/acp-18-13345-2018>,  
659 2018.
- 660 Ohata, S., Mori, T., Kondo, Y., Sharma, S., Hyvärinen, A., Andrews, E., Tunved, P., Asmi, E., Backman, J., Servomaa,  
661 H., Veber, D., Eleftheriadis, K., Vratolis, S., Krejci, R., Zieger, P., Koike, M., Kanaya, Y., Yoshida, A., Moteki, N.,  
662 Zhao, Y., Tobo, Y., Matsushita, J., and Oshima, N.: Estimates of mass absorption cross sections of black carbon for  
663 filter-based absorption photometers in the Arctic, *Atmospheric Measurement Techniques*, 14, 6723–6748,  
664 <https://doi.org/10.5194/amt-14-6723-2021>, 2021.
- 665 Park, K.-T., Yoon, Y. J., Lee, K., Tunved, P., Krejci, R., Ström, J., Jang, E., Kang, H. J., Jang, S., Park, J., Lee, B. Y.,  
666 Traversi, R., Becagli, S., and Hermansen, O.: Dimethyl Sulfide-Induced Increase in Cloud Condensation Nuclei in the  
667 Arctic Atmosphere, *Global Biogeochemical Cycles*, 35, e2021GB006969, <https://doi.org/10.1029/2021GB006969>,  
668 2021.
- 669 Pasquier, J. T., Henneberger, J., Ramelli, F., Lauber, A., David, R. O., Wieder, J., Carlsen, T., Gierens, R., Maturilli,  
670 M., and Lohmann, U.: Conditions favorable for secondary ice production in Arctic mixed-phase clouds, *Atmospheric  
671 Chemistry and Physics*, 22, 15579–15601, <https://doi.org/10.5194/acp-22-15579-2022>, 2022a.
- 672 Pasquier, J. T., David, R. O., Freitas, G., Gierens, R., Gramlich, Y., Haslett, S., Li, G., Schäfer, B., Siegel, K., Wieder,  
673 J., Adachi, K., Belosi, F., Carlsen, T., Decesari, S., Ebell, K., Gilardoni, S., Gysel-Beer, M., Henneberger, J., Inoue, J.,  
674 Kanji, Z. A., Koike, M., Kondo, Y., Krejci, R., Lohmann, U., Maturilli, M., Mazzolla, M., Modini, R., Mohr, C.,  
675 Motos, G., Nenes, A., Nicosia, A., Ohata, S., Paglione, M., Park, S., Pileci, R. E., Ramelli, F., Rinaldi, M., Ritter, C.,  
676 Sato, K., Storelvmo, T., Tobo, Y., Traversi, R., Viola, A., and Zieger, P.: The Ny-Ålesund Aerosol Cloud Experiment  
677 (NASCENT): Overview and First Results, *Bulletin of the American Meteorological Society*, 1,  
678 <https://doi.org/10.1175/BAMS-D-21-0034.1>, 2022b.
- 679 Petters, M. D. and Kreidenweis, S. M.: A single parameter representation of hygroscopic growth and cloud  
680 condensation nucleus activity, *Atmospheric Chemistry and Physics*, 7, 1961–1971, 2007.
- 681 Platt, S. M., Hov, Ø., Berg, T., Breivik, K., Eckhardt, S., Eleftheriadis, K., Evangeliou, N., Fiebig, M., Fisher, R.,  
682 Hansen, G., Hansson, H.-C., Heintzenberg, J., Hermansen, O., Heslin-Rees, D., Holmén, K., Hudson, S., Kallenborn,  
683 R., Krejci, R., Krognes, T., Larssen, S., Lowry, D., Lund Myhre, C., Lunder, C., Nisbet, E., Nizzetto, P. B., Park, K.-  
684 T., Pedersen, C. A., Aspö Pfaffhuber, K., Röckmann, T., Schmidbauer, N., Solberg, S., Stohl, A., Ström, J., Svendby,  
685 T., Tunved, P., Tørnkvist, K., van der Veen, C., Vratolis, S., Yoon, Y. J., Yttri, K. E., Zieger, P., Aas, W., and Tørseth,  
686 K.: Atmospheric composition in the European Arctic and 30 years of the Zeppelin Observatory, Ny-Ålesund,  
687 *Atmospheric Chemistry and Physics*, 22, 3321–3369, <https://doi.org/10.5194/acp-22-3321-2022>, 2022.



- 688 Pöhlker, M. L., Zhang, M., Campos Braga, R., Krüger, O. O., Pöschl, U., and Ervens, B.: Aitken mode particles as  
689 CCN in aerosol- and updraft-sensitive regimes of cloud droplet formation, *Clouds and Precipitation/Atmospheric*  
690 *Modelling/Troposphere/Physics (physical properties and processes)*, <https://doi.org/10.5194/acp-2021-221>, 2021.
- 691 Rahn, K. A.: Relative importances of North America and Eurasia as sources of arctic aerosol, *Atmospheric*  
692 *Environment* (1967), 15, 1447–1455, [https://doi.org/10.1016/0004-6981\(81\)90351-6](https://doi.org/10.1016/0004-6981(81)90351-6), 1981.
- 693 Ramelli, F., Beck, A., Henneberger, J., and Lohmann, U.: Using a holographic imager on a tethered balloon system for  
694 microphysical observations of boundary layer clouds, *Atmospheric Measurement Techniques*, 13, 925–939,  
695 <https://doi.org/10.5194/amt-13-925-2020>, 2020.
- 696 Rantanen, M., Karpechko, A. Y., Lipponen, A., Nordling, K., Hyvärinen, O., Ruosteenoja, K., Vihma, T., and  
697 Laaksonen, A.: The Arctic has warmed nearly four times faster than the globe since 1979, *Commun Earth Environ*, 3,  
698 1–10, <https://doi.org/10.1038/s43247-022-00498-3>, 2022.
- 699 Rastak, N., Silvergren, S., Zieger, P., Wideqvist, U., Ström, J., Svenningsson, B., Maturilli, M., Tesche, M., Ekman,  
700 A. M. L., Tunved, P., and Riipinen, I.: Seasonal variation of aerosol water uptake and its impact on the direct radiative  
701 effect at Ny-Ålesund, Svalbard, *Atmospheric Chemistry and Physics*, 14, 7445–7460, <https://doi.org/10.5194/acp-14-7445-2014>, 2014.
- 703 Reutter, P., Su, H., Trentmann, J., Simmel, M., Rose, D., Gunthe, S. S., Wernli, H., Andreae, M. O., and Pöschl, U.:  
704 Aerosol- and updraft-limited regimes of cloud droplet formation: influence of particle number, size and hygroscopicity  
705 on the activation of cloud condensation nuclei (CCN), *Atmospheric Chemistry and Physics*, 9, 7067–7080,  
706 <https://doi.org/10.5194/acp-9-7067-2009>, 2009.
- 707 Seinfeld, J. H., Bretherton, C., Carslaw, K. S., Coe, H., DeMott, P. J., Dunlea, E. J., Feingold, G., Ghan, S., Guenther,  
708 A. B., Kahn, R., Kraucunas, I., Kreidenweis, S. M., Molina, M. J., Nenes, A., Penner, J. E., Prather, K. A., Ramanathan,  
709 V., Ramaswamy, V., Rasch, P. J., Ravishankara, A. R., Rosenfeld, D., Stephens, G., and Wood, R.: Improving our  
710 fundamental understanding of the role of aerosol–cloud interactions in the climate system, *Proceedings of the National*  
711 *Academy of Sciences*, 113, 5781–5790, <https://doi.org/10.1073/pnas.1514043113>, 2016.
- 712 Shupe, M. D. and Intrieri, J. M.: Cloud Radiative Forcing of the Arctic Surface: The Influence of Cloud Properties,  
713 Surface Albedo, and Solar Zenith Angle, *Journal of Climate*, 17, 616–628, [https://doi.org/10.1175/1520-0442\(2004\)017<0616:CRFOTA>2.0.CO;2](https://doi.org/10.1175/1520-0442(2004)017<0616:CRFOTA>2.0.CO;2), 2004.
- 715 Shupe, M. D., Daniel, J. S., Boer, G. de, Eloranta, E. W., Kollias, P., Long, C. N., Luke, E. P., Turner, D. D., and  
716 Verlinde, J.: A Focus On Mixed-Phase Clouds: The Status of Ground-Based Observational Methods, *Bulletin of the*  
717 *American Meteorological Society*, 89, 1549–1562, <https://doi.org/10.1175/2008BAMS2378.1>, 2008.
- 718 Siegel, K., Neuberger, A., Karlsson, L., Zieger, P., Mattsson, F., Duplessis, P., Dada, L., Daellenbach, K., Schmale, J.,  
719 Baccarini, A., Krejci, R., Svenningsson, B., Chang, R., Ekman, A. M. L., Riipinen, I., and Mohr, C.: Using Novel  
720 Molecular-Level Chemical Composition Observations of High Arctic Organic Aerosol for Predictions of Cloud  
721 Condensation Nuclei, *Environ. Sci. Technol.*, 56, 13888–13899, <https://doi.org/10.1021/acs.est.2c02162>, 2022.
- 722 Sotiropoulou, G., Tjernström, M., Sedlar, J., Achtert, P., Brooks, B. J., Brooks, I. M., Persson, P. O. G., Prytherch, J.,  
723 Salisbury, D. J., Shupe, M. D., Johnston, P. E., and Wolfe, D.: Atmospheric Conditions during the Arctic Clouds in  
724 Summer Experiment (ACSE): Contrasting Open Water and Sea Ice Surfaces during Melt and Freeze-Up Seasons,  
725 *Journal of Climate*, 29, 8721–8744, <https://doi.org/10.1175/JCLI-D-16-0211.1>, 2016.

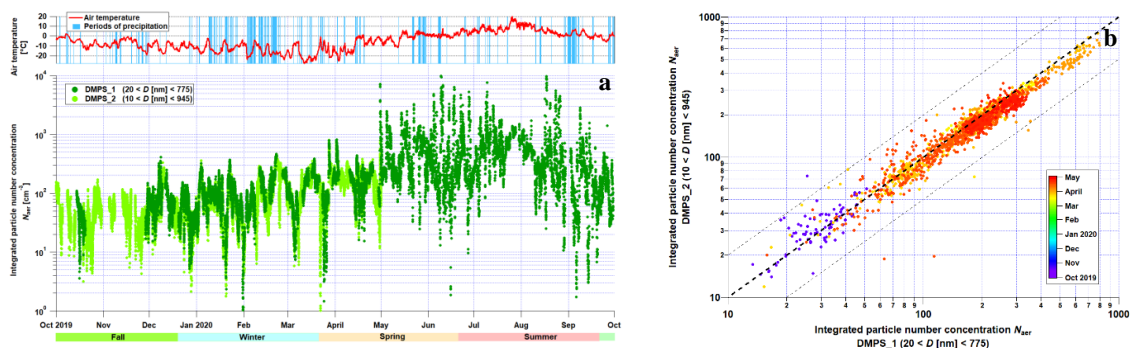




- 726 Ström, J., Umegård, J., Tørseth, K., Tunved, P., Hansson, H.-C., Holmén, K., Wismann, V., Herber, A., and König-  
727 Langlo, G.: One year of particle size distribution and aerosol chemical composition measurements at the Zeppelin  
728 Station, Svalbard, March 2000–March 2001, *Physics and Chemistry of the Earth, Parts A/B/C*, 28, 1181–1190,  
729 <https://doi.org/10.1016/j.pce.2003.08.058>, 2003.
- 730 Ström, J., Engvall, A. C., Delbart, F., Krejci, R., and Treffeisen, R.: On small particles in the Arctic summer boundary  
731 layer: observations at two different heights near Ny-Ålesund, Svalbard, *Tellus B: Chemical and Physical Meteorology*,  
732 61, 473–482, <https://doi.org/10.1111/j.1600-0889.2009.00412.x>, 2009.
- 733 Tan, I. and Storelvmo, T.: Evidence of Strong Contributions From Mixed-Phase Clouds to Arctic Climate Change,  
734 *Geophysical Research Letters*, 46, 2894–2902, <https://doi.org/10.1029/2018GL081871>, 2019.
- 735 Tjernström, M., Leck, C., Birch, C. E., Bottenheim, J. W., Brooks, B. J., Brooks, I. M., Bäcklin, L., Chang, R. Y.-W.,  
736 de Leeuw, G., Di Liberto, L., de la Rosa, S., Granath, E., Graus, M., Hansel, A., Heintzenberg, J., Held, A., Hind, A.,  
737 Johnston, P., Knulst, J., Martin, M., Matrai, P. A., Mauritsen, T., Müller, M., Norris, S. J., Orellana, M. V., Orsini, D.  
738 A., Paatero, J., Persson, P. O. G., Gao, Q., Rauschenberg, C., Ristovski, Z., Sedlar, J., Shupe, M. D., Sierau, B.,  
739 Sirevaag, A., Sjogren, S., Stetzer, O., Swietlicki, E., Szczodrak, M., Vaattovaara, P., Wahlberg, N., Westberg, M., and  
740 Wheeler, C. R.: The Arctic Summer Cloud Ocean Study (ASCOS): overview and experimental design, *Atmospheric  
741 Chemistry and Physics*, 14, 2823–2869, <https://doi.org/10.5194/acp-14-2823-2014>, 2014.
- 742 Touloupas, G., Lauber, A., Henneberger, J., Beck, A., and Lucchi, A.: A convolutional neural network for classifying  
743 cloud particles recorded by imaging probes, *Atmospheric Measurement Techniques*, 13, 2219–2239,  
744 <https://doi.org/10.5194/amt-13-2219-2020>, 2020.
- 745 Tunved, P., Ström, J., and Krejci, R.: Arctic aerosol life cycle: linking aerosol size distributions observed between  
746 2000 and 2010 with air mass transport and precipitation at Zeppelin station, Ny-Ålesund, Svalbard, *Atmospheric  
747 Chemistry and Physics*, 13, 3643–3660, <https://doi.org/10.5194/acp-13-3643-2013>, 2013.
- 748 Turpin, B. J. and Lim, H.-J.: Species Contributions to PM<sub>2.5</sub> Mass Concentrations: Revisiting Common Assumptions  
749 for Estimating Organic Mass, *Aerosol Science and Technology*, 35, 602–610,  
750 <https://doi.org/10.1080/02786820119445>, 2001.
- 751 Twomey, S.: *Radiative properties of clouds*, Univ of Arizona Press, United States, 1993.
- 752 Vincent, W. F.: Arctic Climate Change: Local Impacts, Global Consequences, and Policy Implications, in: *The  
753 Palgrave Handbook of Arctic Policy and Politics*, edited by: Coates, K. S. and Holroyd, C., Springer International  
754 Publishing, Cham, 507–526, [https://doi.org/10.1007/978-3-030-20557-7\\_31](https://doi.org/10.1007/978-3-030-20557-7_31), 2020.
- 755 von der Weiden, S.-L., Drewnick, F., and Borrmann, S.: Particle Loss Calculator – a new software tool for the  
756 assessment of the performance of aerosol inlet systems, *Atmospheric Measurement Techniques*, 2, 479–494,  
757 <https://doi.org/10.5194/amt-2-479-2009>, 2009.
- 758 Zábori, J., Rastak, N., Yoon, Y. J., Riipinen, I., and Ström, J.: Size-resolved cloud condensation nuclei concentration  
759 measurements in the Arctic: two case studies from the summer of 2008, *Atmospheric Chemistry and Physics*, 15,  
760 13803–13817, <https://doi.org/10.5194/acp-15-13803-2015>, 2015.
- 761 Zieger, P., Fierz-Schmidhauser, R., Gysel, M., Ström, J., Henne, S., Yttri, K. E., Baltensperger, U., and Weingartner,  
762 E.: Effects of relative humidity on aerosol light scattering in the Arctic, *Atmospheric Chemistry and Physics*, 10, 3875–  
763 3890, <https://doi.org/10.5194/acp-10-3875-2010>, 2010.

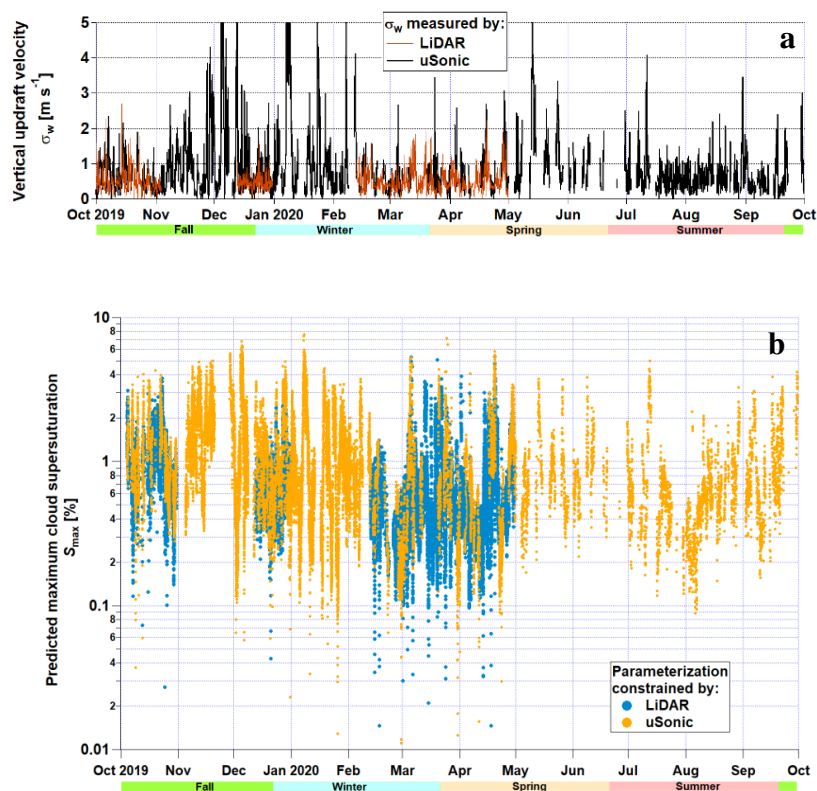


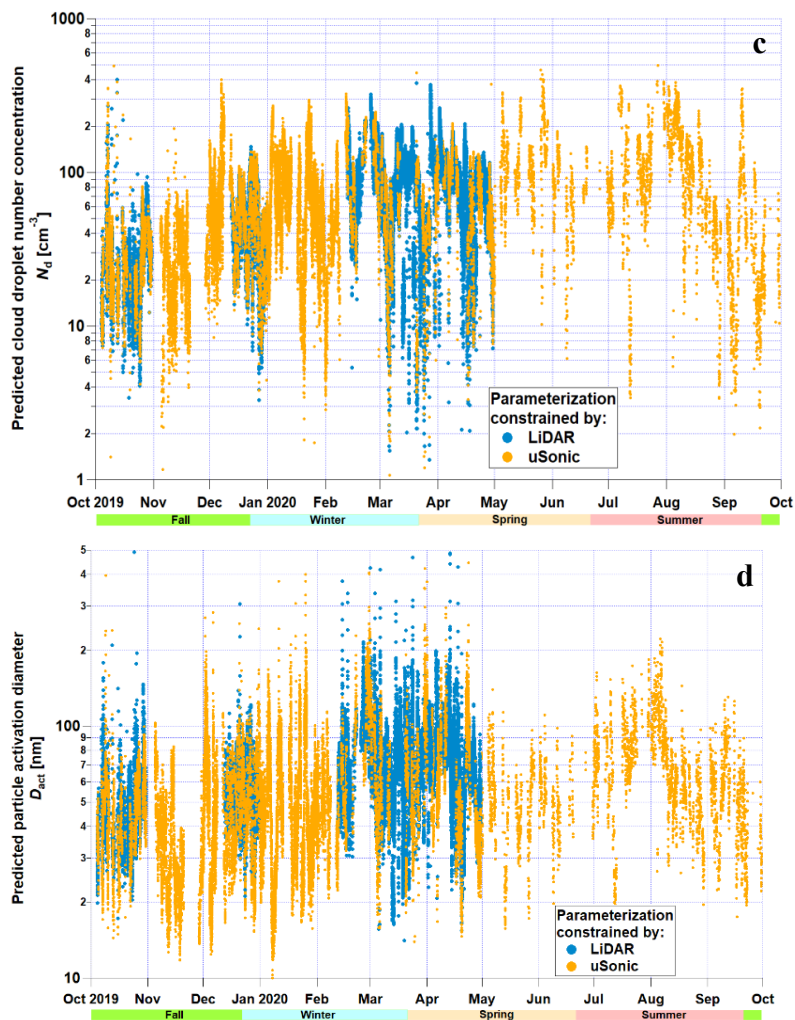
764 Zieger, P., Väisänen, O., Corbin, J. C., Partridge, D. G., Bastelberger, S., Mousavi-Fard, M., Rosati, B., Gysel, M.,  
 765 Krieger, U. K., Leck, C., Nenes, A., Riipinen, I., Virtanen, A., and Salter, M. E.: Revising the hygroscopicity of  
 766 inorganic sea salt particles, Nat Commun, 8, 15883, https://doi.org/10.1038/ncomms15883, 2017.  
 767



768  
 769 **Figure 1:** a): Air temperature measured by a probe (top panel) and integrated particle number concentration  $N_{aer}$  (bottom  
 770 panel) as measured by two DMPS systems at the Zeppelin station, displayed as time series. It should be noted that the two  
 771 DMPSs have different size ranges: 20 to 775 nm for DMPS\_1; 10 to 945 nm for DMPS\_2. b): Comparison of integrated  
 772 particle number concentration  $N_{aer}$  as measured by two differential mobility particle sizer (DMPS) systems at Zeppelin, with  
 773 the date as colour scale.

774  
 775  
 776





777

778

779

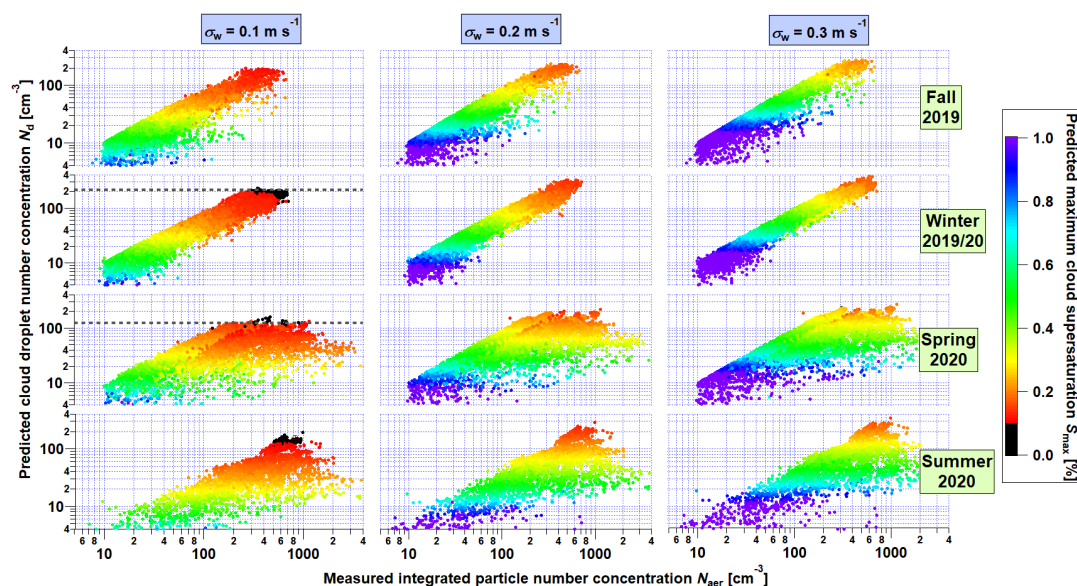
780

781

782

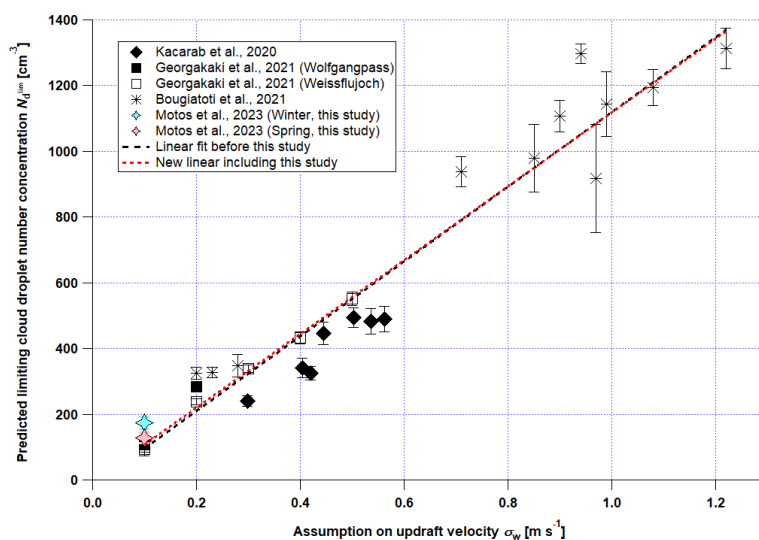
783

Figure 2. Time series of a) measured updraft velocity  $\sigma_w$ , predicted potential b) maximum cloud supersaturation  $S_{max}$ , c) cloud droplet number concentration  $N_d$  and d) particle activation diameter  $D_{act}$  at the Zeppelin station over the whole NASCENT campaign.  $N_d$ ,  $S_{max}$  and  $D_{act}$  are constrained by measurements of  $\sigma_w$ , whose values (after analysis as described in Sect 3.2) are shown at the top of both panels. These results are direct outputs of the cloud droplet formation parameterization presented in Sect. 3.2.



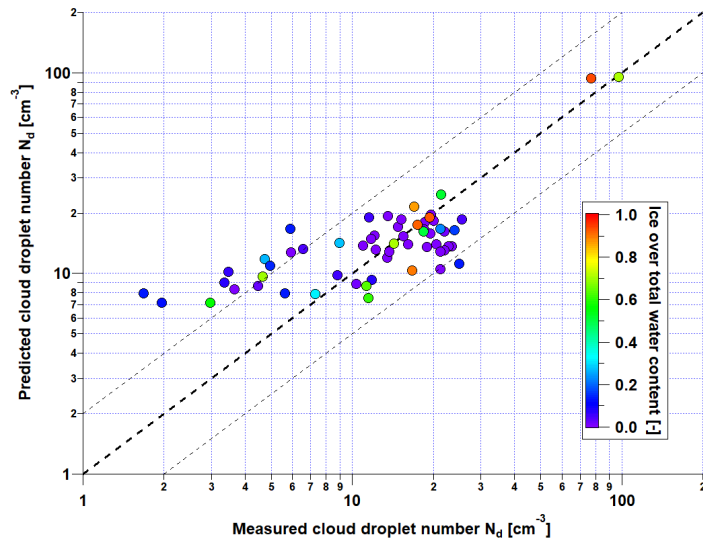
784  
785  
786  
787  
788  
789  
790

Figure 3. Predicted potential droplet number concentration  $N_d$ , an output of the cloud droplet formation parameterization, as a function of integrated particle number concentration  $N_{aer}$ , measured by the DMPSS, split between 12 panels corresponding to four seasons and three different assumptions on updraft velocity  $\sigma_w$ : 0.1, 0.2 and 0.3  $\text{m s}^{-1}$ . The colour scale is the maximum predicted cloud supersaturation  $S_{max}$ ; note that data points for which  $S_{max} < 0.1\%$  are shown in black. Plateau values of  $N_d^{lim}$ , calculated as the average value of data points for which  $S_{max} < 0.1\%$ , are displayed as grey dotted lines.



791  
792  
793  
794

Figure 4. Predicted limiting cloud droplet number concentration plotted against the corresponding assumption on the updraft velocity, comparing the present study with existing literature. The linear fit displayed in black is the one given by Georgakaki et al. (2021); the red one includes results from the current study.



795  
796  
797

Figure 5. Scatterplot of predicted against measured cloud droplet number  $N_d$  during 9 HoloBalloon flights on November 10, 11, 12 2019 and April 1st, 2020.